Evidence of direct electronic band gap in two-dimensional van der Waals indium selenide crystals

Hugo Henck,[1] Debora Pierucci,[2] Jihene Zribi,[1] Federico Bisti,[2] Evangelos Papalazarou,[3] Jean-Christophe Girard,[1] Julien Chaste,[1] François Bertran,[4] Patrick Le Fèvre,[4] Fausto Sirotti,[5] Luca Perfetti,[6] Christine Giorgetti,[6] Abhay Shukla,[7] Julien E. Rault,[4] and Abdelkarim Ouerghi[1]

[1]*Centre de Nanosciences et de Nanotechnologies, Centre National de la Recherche Scientifique, Université Paris-Sud, Université Paris-Saclay, C2N-Marcoussis, 91460 Marcoussis, France*

[2]*CELLS-ALBA Synchrotron Radiation Facility, Carrer de la Llum 2-26, 08290 Cerdanyola del Valles, Barcelona, Spain*

[3]*Laboratoire de Physique des Solides, Centre National de la Recherche Scientifique, Université Paris-Saclay, Université Paris-Sud, 91405 Orsay, France*

[4]*Synchrotron-SOLEIL, Saint-Aubin, BP48, F91192 Gif sur Yvette Cedex, France*

[5]*Laboratoire de Physique de la Matière Condensée, Ecole Polytechnique, Centre National de la Recherche Scientifique, Université Paris Saclay, 91128 Palaiseau Cedex, France*

[6]*Laboratoire des Solides Irradiés, Ecole Polytechnique, Centre National de la Recherche Scientifique, CEA, Université Paris-Saclay, 91128 Palaiseau Cedex, France*

[7]*Institut de Minéralogie de Physique des Matériaux et de Cosmochimie, Sorbonne Universités, UPMC Université Paris 06, UMR Centre National de la Recherche Scientifique 7590, Muséum National d'Histoire Naturelle, IRD UMR 206, 4 Place Jussieu, 75005 Paris, France*

(Received 12 December 2018; published 25 March 2019)

Metal monochalcogenide compounds offer a large variety of electronic properties depending on chemical composition, number of layers, and stacking order. Among them, the InSe has attracted much attention due to the promise of outstanding electronic properties, attractive quantum physics, and high photoresponse. Precise experimental determination of the electronic structure of InSe is sorely needed for better understanding of potential properties and device applications. Here, combining scanning tunneling spectroscopy (STS) and two-photon photoemission spectroscopy, we demonstrate that InSe exhibits a direct band gap of about 1.25 eV located at the Γ point of the Brillouin zone. STS measurements underline the presence of a finite and almost constant density of states (DOS) near the conduction-band minimum. This particular DOS is generated by a poorly dispersive nature of the top valence band, as shown by angle-resolved photoemission spectroscopy (ARPES) investigation. In fact, a hole effective mass of about $m^*/m_0 = -0.95$ ($\overline{\Gamma K}$ direction) was measured. Moreover, using ARPES measurements a spin-orbit splitting of the deeper-lying bands of about 0.35 eV was evidenced. These findings allow a deeper understanding of the InSe electronic properties underlying the potential of III-VI semiconductors for electronic and photonic technologies.

DOI: 10.1103/PhysRevMaterials.3.034004

I. INTRODUCTION

Metal (M) monochalcogenide (X) III-VI compounds (MX), such as InSe, GaSe, GaS, and GaTe, have emerged as promising two-dimensional (2D) semiconductors [1–6]. Their crystal structure consists of covalently bound "X-M-M-X" sheets, stacked vertically through van der Waals (vdW) interaction [7–9]. The electronic band structure of many 2D vdW materials changes as the thickness is reduced down to a few layers [10]. One well-known example is the indirect to direct gap transition that occurs at monolayer (ML) thickness of Mo and W transition-metal dichalcogenides (TMDs) [11]. To date, a wide variety of 2D vdW crystals such as TMDs and hexagonal boron nitride (hBN) have been investigated and exploited as single crystals or in combination with graphene to create functional devices [12–15].

At odds with the dichalcogenide (MX_2) compounds, MX compounds (e.g., GaSe and InSe) are direct-band-gap semiconductors in the bulk (2.1 and 1.2 eV) but they evolve to be indirect band gap when thinned down to few layers [16–18]. Being optically active in the infrared or visible range is a significant advantage for 2D materials since graphene (gapless) and hexagonal boron nitride (>5 eV) are not very practical for optoelectronic applications. The indirect-band-gap transition has not deterred the successful use of few-ML GaSe and InSe as fast photodetectors [19–22]. This kind of indirect-band-gap transition is also a subject of unusual physics, where a near flat valence band pinches down at the Γ point ("Mexican hat") and creates a Van Hove singularity close to the valence-band maximum (VBM) [23]. This peculiar density-of-states (DOS) singularity could lead to interesting effects such as tunable magnetism depending on the doping of the single layer or other instabilities [24,25]. Some recent works highlight the potential applications of InSe and related III-VI 2D materials in optoelectronics [4,18]. Tamalampudi *et al.* [26] showed that devices based on few-layer InSe obtained by mechanical exfoliation can be used as photosensors with high photoresponsivity. Additionally, electroluminescence was observed in the vertically stacked InSe/GaSe heterojunction based on the mechanical exfoliation method of 2D vdW materials [27]. Moreover, such a heterojunction of layered semiconductors where the top and the bottom of the valence band are located close to the Γ point can be very useful in the building of finely tuned artificial semiconductors [28]. In terms of an

 ©2019 American Physical Society

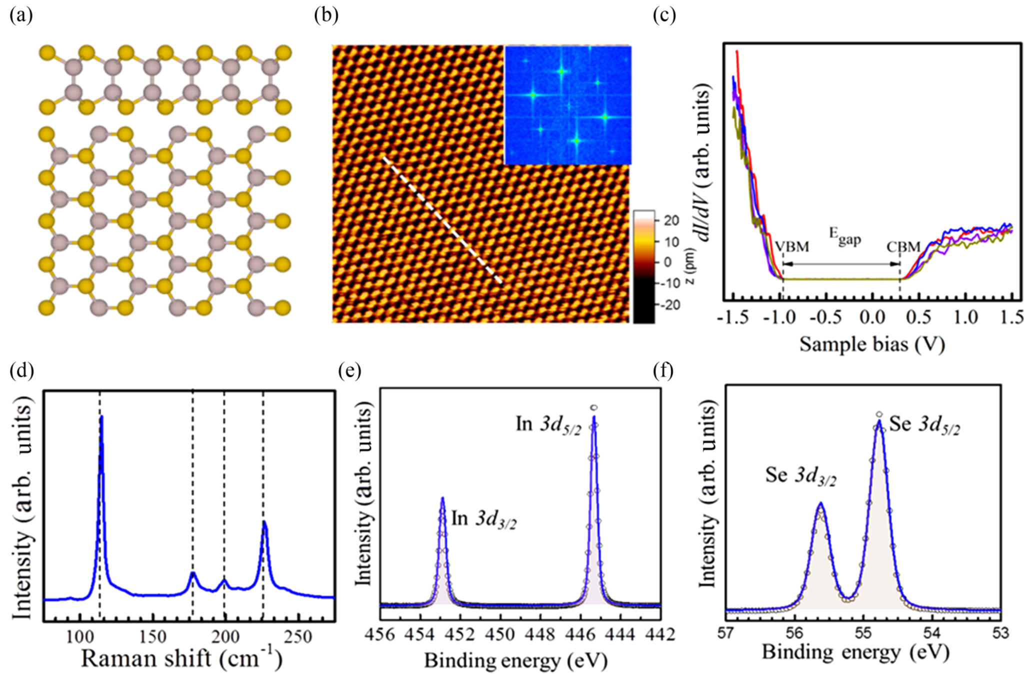

FIG. 1. (a) A schematic diagram of the side view and top view of the hexagonal structure of InSe (the gray spheres refer to indium atoms and the yellow spheres refer to the selenium atoms). (b) Typical STM image (10 × 10 nm) of InSe ($V_{\mathrm{Tip}} = 1.3\,\mathrm{eV}$, $I_t = 400\,\mathrm{pA}$, $T = 4\,\mathrm{K}$). (c) STS dI/dV spectra, taken along the white path in figure (b), showing the electronic band gap of InSe. (d) The characteristic micro-Raman spectrum of ε-InSe crystal. (e, f) High-resolution XPS of InSe at $hn = 600\,\mathrm{eV}$: (e) In $3d$ and (f) Se $3d$.

electrical transport device, it was recently showed that in a InSe field effect transistor (FET) capped with hBN operating at room temperature the carrier mobility can be improved up to $\sim 10^3\,\mathrm{cm}^2/(\mathrm{Vs})$, getting close to the high Hall mobility value of the InSe bulk, which is also well above that of the TMDs [1]. These high-quality devices have also aided the realization of gate-controlled quantum dots in the Coulomb blockade regime with few-layer InSe [29].

Although optical and transport studies of *MX* have made rapid progress, the intrinsic electronic structure is still not precisely understood with many open questions. For example, do *MX* semiconductors have a direct band gap at the Γ points? Fortunately, angle-resolved photoemission spectroscopy (ARPES), scanning tunneling microscopy (STM), and scanning tunneling spectroscopy (STS) have the potential to answer these questions. We report here a detailed experimental study of InSe electronic band structure. ARPES was used to investigate the InSe band structure and the position of the valence-band maximum relative to the Fermi level. This information coupled with the two-photon photoemission spectroscopy (2PPE) and STS measurements gives the band offsets and the electronic band gap in our crystal. Complementary micro-Raman spectroscopy analysis was conducted to study the structural properties of the crystal, exploring the vibration frequencies of phonons corresponding to the characteristic vibrational modes of InSe.

II. RESULTS AND DISCUSSION

Similarly to GaSe, InSe is a layered crystal with strong covalent in-plane interatomic bonding and weaker vdW interplane bonding. A single layer (ML) of InSe consists of four hexagonally arranged atoms linked via covalent bonds in the sequence Se-In-In-Se, with thickness of about 0.8 nm [5] [Fig. 1(a)]. In bulk, these individual InSe layers are held together by vdW forces [30]. Here, high-quality InSe single crystals were synthesized by the flux method [31–33]. In order to study the structural and electronic properties of our sample, we carried out STM and STS measurements at a low temperature of 4.2 K. An atomic lattice image, as shown in Fig. 1(b), can be observed on the InSe sample. The Fourier transform (FT) of the STM images is shown in the inset of Fig. 1(b): the surface exhibits clearly one-ordered structures with the (1×1) symmetry of the InSe. From the FT, it is possible to measure the spatial periodicity of $a = 0.40\,\mathrm{nm}$ in the InSe sample. The resolved differential conductance (dI/dV) spectroscopy versus bias voltage spectra, proportional to the local density of states, measured in different positions of the InSe sample is shown in Fig. 1(c). The VBM is located at $0.96 \pm 0.05\,\mathrm{eV}$ below the Fermi level (i.e., zero bias on the dI/dV spectra), and the conduction-band minimum (CBM) is located at $0.29 \pm 0.03\,\mathrm{eV}$ above the Fermi level, thereby yielding an intrinsic electron quasiparticle band gap of $E_g = 1.25 \pm 0.08\,\mathrm{eV}$. The uncertainty in E_g is the result of the lateral position variations. The relative position of E_F with respect to the band edges reveals n-type doping for our samples which can be attributed to intrinsic point defects such as vacancies and/or lattice antisites, responsible for n doping in other 2D materials [34–36].

In order to probe the chemical and structural properties of synthetic InSe single crystal, micro-Raman and high-resolution x-ray photoemission spectroscopy (HR-XPS) investigations were performed on the same sample. The InSe micro-Raman spectrum measured at room temperature is re-

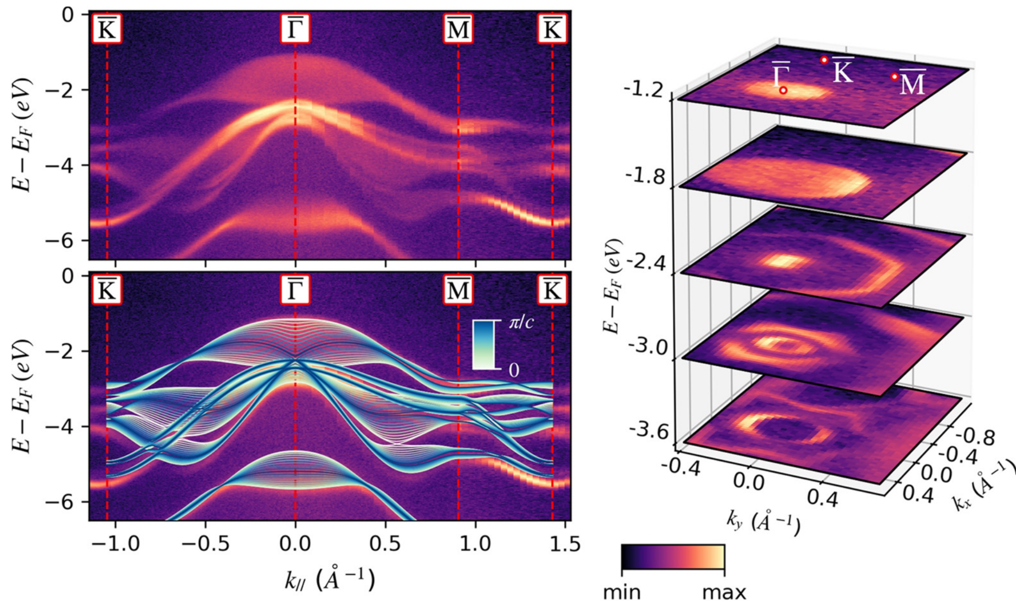

FIG. 2. (a) High-resolution map of the electronic band structure of InSe crystals collected at $h\nu = 60$ eV and $T = 50$ K along the $\overline{K\Gamma MK}$ direction where the Fermi level is located at the zero of the binding energy (top) and comparison between the experimental and the theoretical band structure of InSe in white-blue color scale showing the evolution of the band structure from $k_z = 0$ to π/c (bottom). (b) Isoenergy contours along the $\overline{\Gamma KM}$ plane.

ported in Fig. 1(d). We can distinguish from this spectrum the typical vibrational modes reported previously for bulk InSe [37–39] in nonresonant conditions (laser excitation 532 nm): the peaks at 114.3, 177.8, and 226.9 cm^{-1} corresponding, respectively, to the vibrational modes A^1_{1g}, E^1_{2g}, and A^2_{1g} [4,6,38,40]. A small peak at around 200 cm^{-1} is also present, a signature of the ε polytype [41–43]. HR-XPS measurements were carried out on the InSe crystals at the Cassiopée beamline of the synchrotron Soleil (France) at 50 K. The overview spectrum on a wide energy range ($h\nu = 600$ eV) (see Fig. S1 of Supplemental Material [44]) shows the only presence of the In (In 3d and In 4d) and Se (Se 3s, Se 3p, and Se 3d) peaks, without any signal related to oxygen or carbon, underlying the absence of contaminations. High-resolution spectra for In (In 3d and In 4d) and Se (Se 3d) are also recorded at 600 eV [see Figs. 1(e), S2 of Supplemental Material [44], and 1(f), respectively). The different components of the spectra were decomposed by a curve fitting procedure (see Sec. I of Supplemental Material [44]). The experimental data are displayed in dots and the blue solid lines represent the envelope of the fitted components. The In 3d spectrum presents two peaks at a binding energy of 445.3 and 452.8 eV, which can be attributed to the In $3d_{5/2}$ and In $3d_{3/2}$ [spin-orbit (SO) splitting of 7.5 eV, with the expected $3d_{3/2} : 3d_{5/2}$ ratio of 0.66]. Similarly, two components are also present for the Se 3d peak, corresponding to the Se $3d_{5/2}$ and $3d_{3/2}$ at 54.7 and 55.5 eV, respectively, with a SO splitting of 0.8 eV and the expected $3d_{3/2} : 3d_{5/2}$ ratio of 0.66. No other components are detected in the spectra related to oxidized InSe (i.e., Se-O around 59 eV) [6,45–47]. The obtained binding-energy values are in agreement with previously reported ones obtained for a single-crystal InSe (n-type doping) [45,48]. Moreover, a quantitative analysis, obtained using the intensity of the In 4d and Se 3d peaks (scaled by the specific photoemission cross section; see Sec. IV of Supplemental Material [44]) [49–52], shows a In:Se ratio of about 1.01, confirming the monochalcogenide phase of the crystal [53].

More insight into the InSe electronic structure was obtained using ARPES combined with density functional theory (DFT) calculations (for more details see Sec. V of Supplemental Material [44]). In Fig. 2(a) top panel, we report the InSe bulk band-structure projection on the surface Brillouin zone (BZ) [see inset of Fig. 2(a) top panel] along the $\overline{K\Gamma MK}$, as explored by using a photon energy of 60 eV. The topmost part of the valence band is characterized by a down-dispersing paraboloid centered at the $\bar{\Gamma}$ point. The VBM is located at -1.05 ± 0.05 eV, in agreement with the STS measurements. As shown by theoretical calculations [54], this paraboloid has a p_z-like symmetry (out-of-plane orbital), which differentiates from the p_x- and p_y-like symmetries (in-plane orbitals) located at higher distance from the Fermi level (about -2.5 eV). The spin-orbit interaction induces an energy splitting of these two latter bands of $\Delta_{SO} = 0.35$ eV (see Fig. S3 of Supplemental Material [44]) [54,55]. Such splitting is of relevance for the higher-energy photoluminescence transitions [56,57]. The large uncertainty of the k_z vector, due to the low photon energy (60 eV) [58], spreads the paraboloid contours to low binding energy [see also Figs. 3(d)–3(f) for the $\overline{K\Gamma}$ direction explored by using the different photon energies]. This effect is more pronounced around $\bar{\Gamma}$ than $\bar{K}$ or $\bar{M}$, due to the lower band dispersion along k_z of the states around the latter points than $\bar{\Gamma}$. In Fig. 2(a) bottom panel, the calculated band structure is superimposed on the experimental data. The excellent agreement confirms we are probing the band structure of the bulk ε-InSe. In white-blue color scale, the evolution of the band structure from $k_z = 0$ to π/c is highlighted. From the projection of the bulk valence band on the surface Brillouin zone ($\overline{\Gamma K}$ direction) of Fig. 2(a) the effective mass of the hole

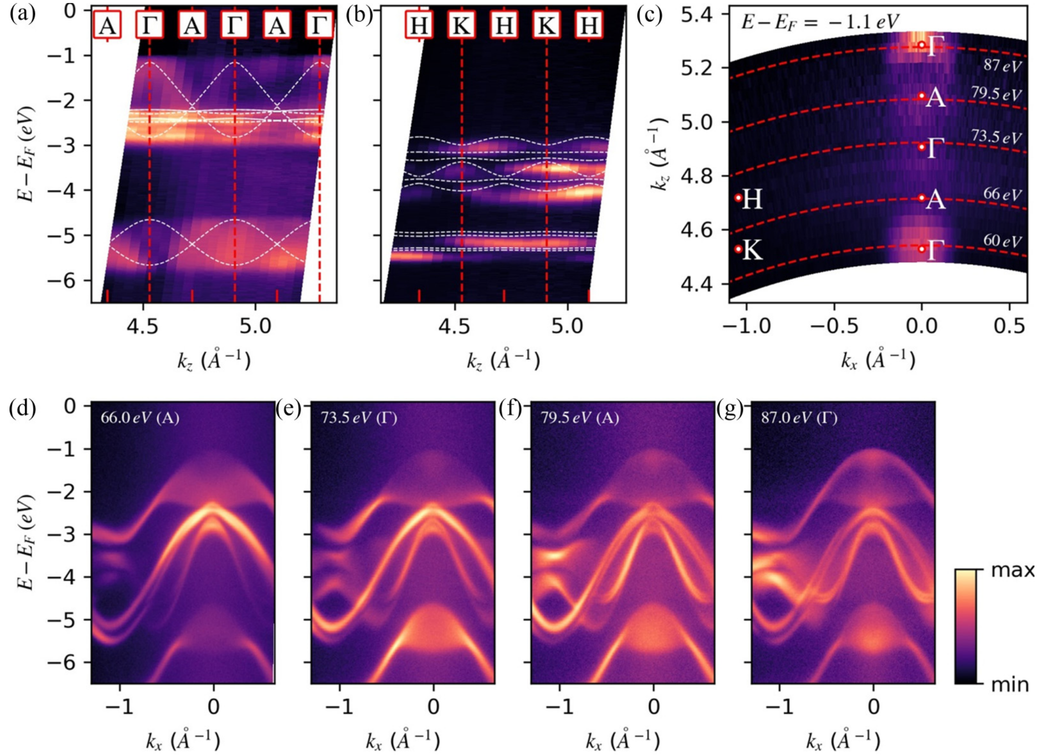

FIG. 3. Photon energy scan (from 58.5 to 88.5 eV): (a) band dispersion along ΓA, (b) band dispersion along KH, and (c) isoenergy contour along the ΓAK plane. The theoretical calculations are represented by white dashed lines. Electronic band structure of InSe along the ($\overline{\Gamma K}$) high-symmetry direction collected at different photon energies ($h\nu = 66$, 73.5, and 87 eV) and $T = 50$ K. Following Fig. 3(c), the reported photon energies are the ones passing, respectively, through the A point and two Γ points.

close to the $\bar{\Gamma}$ point is calculated. The experimental dispersion has been fitted with a parabolic model $E(\boldsymbol{k}) = E_0 + \frac{\hbar^2}{2m^*}\boldsymbol{k}^2$ where m^* is the effective electron mass and $\hbar$ is the reduced Planck constant. We found that the hole effective mass at the $\bar{\Gamma}$ point is about $m^*/m_0 = -0.95 \pm 0.05$. One can notice that this mass is close to m_0, which implies that the InSe band is poorly dispersive. This feature leads to the appearance of a very sharp DOS near the top of the valence band of InSe as observed by STS.

The isoenergy contours in the $\overline{\Gamma KM}$ plane [Fig. 2(b)] confirm the presence of states only around the $\bar{\Gamma}$ point. They show an in-plane isotropic extension of the paraboloid at least until -1.8 eV, reaching a hexagonal shape once approaching the corners of the Brillouin zone at lower binding energy. The in-plane orbitals, instead, establish a star-shaped contour following the surface symmetry. In Figs. 3(a) and 3(b) the out-of-plane direction is explored by a photon energy scan (from 58.5 to 88.5 eV), giving access to the k_z vector (the used inner potential is 19 eV). The band dispersion along ΓA [Fig. 3(a)] shows a broad parabola around Γ points for the topmost part of the valence band (mostly visible around $k_z = 4.5\,\text{Å}^{-1}$) and almost nondispersing features around -2.5 eV (red arrow). These observations are in excellent agreement with the theoretical calculations (white dashed lines in Fig. 3), confirming also the previous assignment of an out-of-plane p_z-like orbital for the topmost part of the valence band and in-plane p_x- and p_y-like orbitals at around -2.5 eV. An additional intensity modulation, following the perpendicular periodicity of the crystal, is also recognizable in the broad band centered at -5.0 eV, suggesting an out-of-plane orbital character for this band. The band dispersion along KH [Fig. 3(b)] is instead showing almost nondispersing features as expected from calculation (white dashed lines), reflecting the in-plane two-dimentional character of the bands around K and H points. To complete the investigation we also show the isoenergy contour in the ΓAK plane [Fig. 3(c)] near the valence-band maximum. This contour confirms the location of the VBM around the Γ points; in fact, almost no signal is present in other places of the BZ. For the photon energies of $h\nu = 66$, 73.5, 79.5, and 87 eV we are passing through two A points and two Γ points. The corresponding band structures for these photon energies are reported in Figs. 3(d)–3(g). The topmost part of the valence band near the first A point (at 66 eV) shows a reduced signal at the center of k_x in favor of an increase on the sides. The signal almost vanishes for the Γ point at 73.5 eV. This reduced signal intensity for the Γ point in the middle of the explored k_z range (around $k_z = 4.8\,\text{Å}^{-1}$), as recognizable also in Figs. 3(a) and 3(c), is due to dipole selection rules in the photoemission process. As in the case of graphite, this signal modulation is following a double periodicity along k_z ($4\pi/c$, instead of $2\pi/c$). Therefore, this effect can be attributed to the constructive and destructive interference of p_z orbitals between the layers of the unit cell [59]. Therefore, it can be considered as a signature of three-dimensionality for the band structure, but also as an indication of good quality for the investigated crystal. The second A point at 79.5 eV is also characterized by reduced intensity, but a small signal is present at the topmost part of the valence

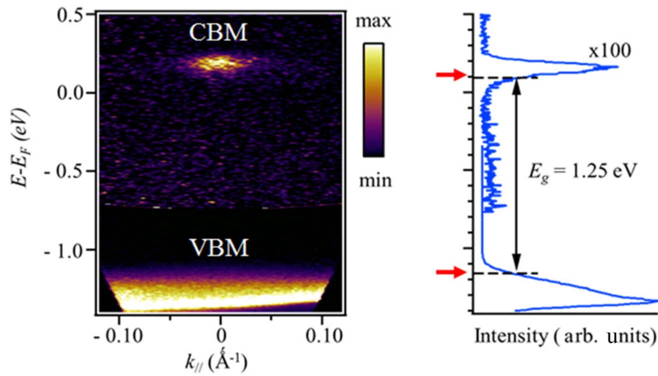

FIG. 4. 2PPE image acquired along the $\overline{\Gamma K}$ direction using 6.24-eV probe and 1.56-eV pump photon energy. An electronic band gap of 1.25 eV at the $\bar{\Gamma}$ point was measured. Red arrows show the VBM and CBM obtained from an energy dispersion curve around $\bar{\Gamma}$. Note that the photoelectron intensity at energy larger than -0.8 has been multiplied by a large factor in order to equalize on the same color scale the signal of the VBM and CBM.

band. Due to the fact that this signal is not dispersing in the k space (either along k_x or along k_z), it can be related to the presence of crystal defects. Finally, the Γ point explored with the highest photon energy (87 eV) shows a reduced spread of the paraboloid contours to low binding energy, due to the reduced uncertainty on the k_z vector [58].

A complete picture of the electronic structure of the InSe crystal is obtained using 2PPE spectroscopy, giving access to the unoccupied state. We used a Ti:sapphire laser system delivering 6-μJ pulses with a repetition rate of 250 kHz. The system was photoexcited using the fundamental beam, $\omega = 1.56\,\text{eV}$ (pump), and probed using the 4ω pulse of 6.24 eV. Figures 4(a) and 4(b) show a 2PPE image acquired along the $\overline{\Gamma K}$ direction at a pump-probe delay of 4 µs to 1 ps. The system displays long electron dynamics, maintaining a large electronic density around +0.1 eV for more than 4 µs. In the image we can observe that the CBM in InSe crystals is located at the Γ point, as the VBM. A single-particle electronic band gap of $E_g = E_{\text{CBM}} - E_{\text{VBM}} = 1.25 \pm 0.04\,\text{eV}$ was measured [Fig. 4(b)], in agreement with the STS spectra. This result suggests that InSe has a direct electronic band gap at the Γ point. Accordingly, pump-probe dynamics performed in this system have shown a dispersion of unoccupied states with the CBM in the center of the Brillouin zone [32].

III. CONCLUSIONS

In summary, we have presented an exhaustive study of the electronic band structure of the InSe crystal combining spectroscopic tools and theoretical investigation (DFT). The joint analysis of the DOS using STS and of the band structure using 2PPE indicates that the InSe crystal presents a direct quasiparticle band gap of about 1.25 eV located at the Γ point of the BZ. ARPES spectra reveal that the spin-orbit interaction lifts band degeneracies in the deeper-lying valence band, causing a splitting of about 0.35 eV. These properties hold greats potential for a wide range of applications of vdW heterostructures based on layered InSe, ranging from thermoelectric applications to nanoelectronic and optoelectronic ones.

ACKNOWLEDGMENTS

We acknowledge funding from the French National Research Agency ANR H2DH (Grant No. ANR-15-CE24-0016), RhomboG (Grant No. ANR-17-CE24-0030), Labex NanoSaclay (Grant No. ANR-10-LABX-0035), and the EU-H2020 research and innovation programme under Grant Agreement No. 654360 having benefitted from the access provided by C2N and Synchrotron SOLEIL in Paris within the framework of the NFFA-Europe Transnational Access Activity. Computer time has been granted by GENCI (Project No. 544).

[1] D. A. Bandurin, A. V. Tyurnina, G. L. Yu, A. Mishchenko, V. Zólyomi, S. V. Morozov, R. K. Kumar, R. V. Gorbachev, Z. R. Kudrynskyi, S. Pezzini, Z. D. Kovalyuk, U. Zeitler, K. S. Novoselov, A. Patanè, L. Eaves, I. V. Grigorieva, V. I. Fal'ko, A. K. Geim, and Y. Cao, Nat. Nanotechnol. **12**, 223 (2016).

[2] V. Zolyomi, N. D. Drummond, and V. I. Fal'Ko, Phys. Rev. B: Condens. Matter Mater. Phys. **87**, 195403 (2013).

[3] G. W. Mudd, M. R. Molas, X. Chen, V. Zólyomi, K. Nogajewski, Z. R. Kudrynskyi, Z. D. Kovalyuk, G. Yusa, O. Makarovsky, L. Eaves, M. Potemski, V. I. Fal'ko, and A. Patanè, Sci. Rep. **6**, 39619 (2016).

[4] Z. Chen, J. Biscaras, and A. Shukla, Nanoscale **7**, 5981 (2015).

[5] G. W. Mudd, A. Patanè, Z. R. Kudrynskyi, M. W. Fay, O. Makarovsky, L. Eaves, Z. D. Kovalyuk, V. Zólyomi, and V. Falko, Appl. Phys. Lett. **105**, 221909 (2014).

[6] Z. Yang, W. Jie, C. H. Mak, S. Lin, H. Lin, X. Yang, F. Yan, S. P. Lau, and J. Hao, ACS Nano **11**, 4225 (2017).

[7] Y. Lee, R. Pisoni, H. Overweg, M. Eich, P. Rickhaus, A. Patane, Z. R. Kudrynskyi, Z. D. Kovalyuk, R. Gorbachev, K. Watanabe, T. Taniguchi, T. Ihn, and K. Ensslin, 2D Mater. **5**, 035040 (2018).

[8] D. J. Terry, V. Zólyomi, M. Hamer, A. V. Tyurnina, D. G. Hopkinson, A. M. Rakowski, S. J. Magorrian, N. Clark, Y. M. Andreev, O. Kazakova, K. Novoselov, S. J. Haigh, V. I. Fal'Ko, and R. Gorbachev, 2D Mater. **5**, 041009 (2018).

[9] N. Balakrishnan, E. D. Steer, E. F. Smith, Z. R. Kudrynskyi, Z. D. Kovalyuk, L. Eaves, A. Patanè, and P. H. Beton, 2D Mater. **5**, 035026 (2018).

[10] A. K. Geim and I. V. Grigorieva, Nature (London) **499**, 419 (2013).

[11] K. F. Mak, C. Lee, J. Hone, J. Shan, and T. F. Heinz, Phys. Rev. Lett. **105**, 136805 (2010).

[12] H. Henck, D. Pierucci, G. Fugallo, J. Avila, G. Cassabois, Y. J. Dappe, M. G. Silly, C. Chen, B. Gil, M. Gatti, F. Sottile, F. Sirotti, M. C. Asensio, and A. Ouerghi, Phys. Rev. B **95**, 085410 (2017).

[13] Y. Deng, Z. Luo, N. J. Conrad, H. Liu, Y. Gong, S. Najmaei, P. M. Ajayan, J. Lou, X. Xu, and P. D. Ye, ACS Nano **8**, 8292 (2014).
[14] W. Kim, C. Li, F. A. Chaves, D. Jiménez, R. D. Rodriguez, J. Susoma, M. A. Fenner, H. Lipsanen, and J. Riikonen, Adv. Mater. **9**, 1845 (2016).
[15] X. Yuan, L. Tang, S. Liu, P. Wang, Z. Chen, C. Zhang, Y. Liu, W. Wang, Y. Zou, C. Liu, N. Guo, J. Zou, P. Zhou, W. Hu, and F. Xiu, Nano Lett. **15**, 3571 (2015).
[16] X. Li, M.-W. Lin, A. A. Puretzky, J. C. Idrobo, C. Ma, M. Chi, M. Yoon, C. M. Rouleau, I. I. Kravchenko, D. B. Geohegan, and K. Xiao, Sci. Rep. **4**, 5497 (2014).
[17] X. Li, L. Basile, B. Huang, C. Ma, J. Lee, I. V Vlassiouk, A. A. Puretzky, M. Lin, M. Yoon, M. Chi, J. C. Idrobo, C. M. Rouleau, B. G. Sumpter, D. B. Geohegan, and K. Xiao, ACS Nano **9**, 8078 (2015).
[18] C. S. Jung, F. Shojaei, K. Park, J. Y. Oh, H. S. Im, D. M. Jang, J. Park, and H. S. Kang, ACS Nano **9**, 9585 (2015).
[19] W. Feng, Z. Jin, J. Yuan, J. Zhang, S. Jia, L. Dong, J. Yoon, L. Zhou, R. Vajtai, and J. M. Tour, 2D Mater. **5**, 025008 (2018).
[20] F. Yan, L. Zhao, A. Patanè, P. Hu, X. Wei, W. Luo, D. Zhang, Q. Lv, Q. Feng, and C. Shen, Nanotechnology **28**, 27LT01 (2017).
[21] S. Lei, F. Wen, L. Ge, S. Najmaei, A. George, Y. Gong, W. Gao, Z. Jin, B. Li, J. Lou, J. Kono, R. Vajtai, P. Ajayan, and N. J. Halas, Nano Lett. **15**, 3048 (2015).
[22] P. Hu, Z. Wen, L. Wang, P. Tan, and K. Xiao, ACS Nano **6**, 5988 (2012).
[23] Z. Ben Aziza, D. Pierucci, H. Henck, M. G. Silly, C. David, M. Yoon, F. Sirotti, K. Xiao, M. Eddrief, J.-C. Girard, and A. Ouerghi, Phys. Rev. B **96**, 035407 (2017).
[24] T. Cao, Z. Li, and S. G. Louie, Phys. Rev. Lett. **114**, 236602 (2015).
[25] Q. Zhang and U. Schwingenschlögl, Phys. Rev. B **97**, 155415 (2018).
[26] S. R. Tamalampudi, Y.-Y. Lu, R. Kumar U., R. Sankar, C.-D. Liao, K. Moorthy B., C.-H. Cheng, F. C. Chou, and Y.-T. Chen, Nano Lett. **14**, 2800 (2014).
[27] M. Buscema, J. O. Island, D. J. Groenendijk, S. I. Blanter, G. A. Steele, H. S. J. van der Zant, and A. Castellanos-Gomez, Chem. Soc. Rev. **44**, 3691 (2015).
[28] E. Ponomarev, N. Ubrig, I. Gutiérrez-Lezama, H. Berger, and A. F. Morpurgo, Nano Lett. **18**, 5146 (2018).
[29] M. Hamer, E. Tóvári, M. Zhu, M. D. Thompson, A. Mayorov, J. Prance, Y. Lee, R. P. Haley, Z. R. Kudrynskyi, A. Patanè, D. Terry, Z. D. Kovalyuk, K. Ensslin, A. V. Kretinin, A. Geim, and R. Gorbachev, Nano Lett. **18**, 3950 (2018).
[30] P. K. Larsen, S. Chiang, and N. V. Smith, Phys. Rev. B **15**, 3200 (1977).
[31] C. De Blasi, G. Micocci, S. Mongelli, and A. Tepore, J. Cryst. Growth **57**, 482 (1982).
[32] Z. Chen, C. Giorgetti, J. Sjakste, R. Cabouat, V. Véniard, Z. Zhang, A. Taleb-Ibrahimi, E. Papalazarou, M. Marsi, A. Shukla, J. Peretti, and L. Perfetti, Phys. Rev. B **97**, 241201 (2018).
[33] A. Chevy, J. Cryst. Growth **67**, 119 (1984).
[34] W. Zhou, X. Zou, S. Najmaei, Z. Liu, Y. Shi, J. Kong, and J. Lou, Nano Lett. **13**, 2615 (2013).
[35] D. Pierucci, H. Henck, J. Avila, A. Balan, C. H. Naylor, G. Patriarche, Y. J. Dappe, M. G. Silly, F. Sirotti, A. T. C. Johnson, M. C. Asensio, and A. Ouerghi, Nano Lett. **16**, 4054 (2016).
[36] D. Pierucci, H. Henck, Z. Ben Aziza, C. H. Naylor, A. Balan, J. E. Rault, M. G. Silly, Y. J. Dappe, F. Bertran, P. Le Fèvre, F. Sirotti, A. T. C. Johnson, and A. Ouerghi, ACS Nano **11**, 1755 (2017).
[37] C. Ulrich, M. A. Mroginsky, A. R. Goni, A. Canterero, U. Schwarz, V. Munoz, and K. Syassen, Phys. Stat. Sol. (B) **198**, 121 (1996).
[38] O. Del Pozo-Zamudio, S. Schwarz, J. Klein, R. C. Schofield, E. a. Chekhovich, O. Ceylan, E. Margapoti, A. I. Dmitriev, G. V. Lashkarev, D. N. Borisenko, N. N. Kolesnikov, J. J. Finley, and A. I. Tartakovskii, arXiv:1506.05619.
[39] J. F. Sánchez-Royo, G. Muñoz-Matutano, M. Brotons-Gisbert, J. P. Martínez-Pastor, A. Segura, A. Cantarero, R. Mata, J. Canet-Ferrer, G. Tobias, E. Canadell, J. Marqués-Hueso, and B. D. Gerardot, Nano Res. **7**, 1556 (2014).
[40] S. Lei, L. Ge, S. Najmaei, A. George, R. Kappera, J. Lou, M. Chhowalla, H. Yamaguchi, G. Gupta, R. Vajtai, A. D. Mohite, and P. M. Ajayan, ACS Nano **8**, 1263 (2014).
[41] Z. Chen, K. Gacem, M. Boukhicha, J. Biscaras, and A. Shukla, Nanotechnology **24**, 415708 (2013).
[42] S. Jandl and C. Carlone, Solid State Commun. **25**, 5 (1978).
[43] C. Carlone and S. Jandl, Solid State Commun. **29**, 31 (1979).
[44] See Supplemental Material at http://link.aps.org/supplemental/10.1103/PhysRevMaterials.3.034004 for methods and characterization (STM/STS, Raman Spectroscopy, and XPS), x-ray photoemission spectroscopy (XPS) measurements, angle resolved photoemission spectroscopy (ARPES) measurements and DFF calculations.
[45] G. Brojerdi, G. Tyuliev, D. Fargues, M. Eddrief, and M. Balkanski, Surf. Interface Anal. **25**, 111 (1997).
[46] J. Lauth, F. E. S. Gorris, M. Samadi Khoshkhoo, T. Chassé, W. Friedrich, V. Lebedeva, A. Meyer, C. Klinke, A. Kornowski, M. Scheele, and H. Weller, Chem. Mater. **28**, 1728 (2016).
[47] I. Miyake, T. Tanpo, and C. Tatsuyama, Jpn. J. Appl. Phys. **23**, 172 (1984).
[48] A. Segura, J. P. Guesdon, J. M. Besson, and A. Chevy, J. Appl. Phys. **54**, 876 (1983).
[49] M. P. Seah, Surf. Interface Anal. **2**, 222 (1980).
[50] M. P. Seah and I. S. Gilmore, Phys. Rev. B **73**, 174113 (2006).
[51] J. T. Grant, Surf. Interface Anal. **14**, 271 (1989).
[52] J. J. Yeh and I. Lindau, At. Data Nucl. Data Tables **32**, 1 (1985).
[53] W. Shi, S. Yu, P. Liu, W. Fan, H. Luo, and S. Song, Chem. Eng. J. **225**, 474 (2013).
[54] D. T. Do, S. D. Mahanti, and C. W. Lai, Sci. Rep. **5**, 17044 (2015).
[55] M. Zhou, R. Zhang, J. Sun, W.-K. Lou, D. Zhang, W. Yang, and K. Chang, Phys. Rev. B **96**, 155430 (2017).
[56] S. J. Magorrian, V. Zólyomi, and V. I. Fal'Ko, Phys. Rev. B **96**, 079905 (2017).
[57] Z. Ben Aziza, V. Zólyomi, H. Henck, D. Pierucci, M. G. Silly, J. Avila, S. J. Magorrian, J. Chaste, C. Chen, M. Yoon, K. Xiao, F. Sirotti, M. C. Asensio, E. Lhuillier, M. Eddrief, V. I. Fal'Ko, and A. Ouerghi, Phys. Rev. B **98**, 115405 (2018).
[58] V. N. Strocov, J. Electron Spectros. Relat. Phenomena **130**, 65 (2003).
[59] F. Matsui, H. Nishikawa, H. Daimon, M. Muntwiler, M. Takizawa, H. Namba, and T. Greber, Phys. Rev. B **97**, 045430 (2018).